THE JOURNAL OF PHYSICAL CHEMISTRY C

Article

Cite This: J. Phys. Chem. C 2019, 123, 15195−15203

pubs.acs.org/JPCC

Roles of Superchirality and Interference in Chiral Plasmonic Biodetection

Cameron Gilroy,*[,†] Shun Hashiyada,*[,‡,∥] Kensaku Endo,[§] Affar S. Karimullah,[†] Laurence D. Barron,[†] Hiromi Okamoto,[‡] Yoshihiko Togawa,[§] and Malcolm Kadodwala*[,†]

[†]School of Chemistry, University of Glasgow, Joseph Black Building, Glasgow G12 8QQ, U.K.

[‡]Institute for Molecular Science and The Graduate University for Advanced Studies (Sokendai), 38 Nishigonaka, Myodaiji, Okazaki, Aichi 444-8585, Japan

[§]Department of Physics and Electronics, Osaka Prefecture University, Sakai 599-8570, Japan

[∥]Innovative Photon Manipulation Research Team, RIKEN Center for Advanced Photonics, Wako, Saitama 351-0198, Japan

S *Supporting Information*

ABSTRACT: Chiral plasmonic nanostructures enable ≤pg detection and characterization of biomaterials. The sensing capabilities are associated with the chiral asymmetry of the near fields, which locally can be greater than equivalent circularly polarized light, a property referred to as superchirality. However, sensing abilities do not simply scale with the magnitude of superchirality. We show that chiral molecular sensing is correlated to the thickness of a nanostructure. This observation is reconciled with a previously unconsidered interference mechanism for the sensing phenomenon. It involves the "dissipation" of optical chirality into chiral material currents through the interference of fields generated by two spatially separated chiral modes. The presence of a chiral dielectric causes an asymmetric change in the phase difference, resulting in asymmetric changes to chiroptical properties. Thus, designing a chiral plasmonic sensor requires engineering a substrate that can sustain both superchiral fields and an interference effect.

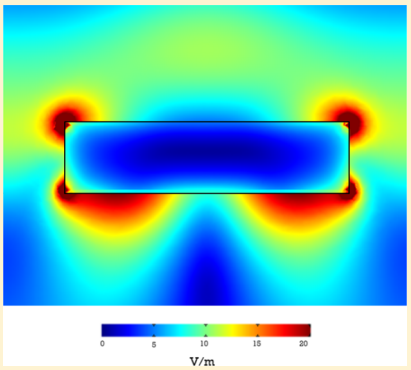

INTRODUCTION

The detection and characterization of inherently chiral biological materials is of both fundamental and practical interest, with applications in life and analytical sciences. Routinely, this is achieved using chirally sensitive spectroscopic techniques which are based on the differential interaction of circularly polarized light (CPL), such as circular dichroism (CD) and optical rotatory dispersion (ORD).[1,2] Because of the inherent weakness of the asymmetric interaction of CPL, chiroptical techniques require relatively large amounts of samples, that is, ≥μg.[3] This precludes the use of these chiroptical techniques for applications for which ultrasensitivity (<pg) is required, such as biosensing. Recently, it has been demonstrated that chiral near fields generated by optical excitation of chiral plasmonic nanostructures can be used for ultrasensitive detection and structural characterization of biomaterials. The presence of chiral dielectric materials, such as biomacromolecules, within the near-field region induces asymmetric changes in the optical properties (CD, ORD, and reflectance spectra) of chiral plasmonic nanostructures.[4−9]

The origin of this asymmetry is undoubtedly the chiral asymmetry of the near fields generated around the nanostructures. The chiral asymmetry of the near fields can be parameterized using an optical chirality factor.[10−12] In localized regions, around the nanostructure, the near fields can have greater optical chirality than the equivalent CPL, and this effect has been termed "*superchirality*".[11] It has been assumed that by optimizing the level of the enhanced optical chirality, sensing effects can be maximized.[13] However, the sensing capability of chiral near fields is not a generic phenomenon. Some structures which are predicted to have near fields with very high local optical chiralities show very weak sensing capabilities.[14] In this study, we present evidence that suggests that the sensing capability of a chiral structure is correlated to a chiral dielectric-induced asymmetry in the capacities of left- and right-handed forms to convert the chirality of light into chiral surface charge distributions, a process referred to as the dissipation of optical chirality.[15,16] To account for this asymmetry, we propose a previously unconsidered mechanism of optical chirality dissipation based on the interference between chiral fields generated by spatially separated sources. The far field photon (energy) fluxes, which are monitored to obtain extinction spectra, have contributions because of absorption and scattering. Thus, by analogy, we propose the hypothesis that optical chirality, a conserved quantity like energy, is dissipated through both absorption and scattering. Dissipation through scattering is structurally dependent and strongly influenced by the presence of the surrounding chiral

Received: March 25, 2019
Revised: May 23, 2019
Published: May 28, 2019

dielectric. This latter property is the origin of previously reported biosensing capabilities. In the system described in this study, optical chirality dissipation occurs through the interference of fields generated by two spatially separated chiral modes. The presence of a chiral dielectric (molecules) has an asymmetric influence on the phase difference between the two sources of chiral fields, leading to an asymmetry in the level of conversion of optical chirality to chiral material currents. This leads to an asymmetric change in the (chir)optical properties of plasmonic structures. Thus, our work provides the starting point for the development of a design framework to optimize the sensing capabilities of chiral plasmonic structures.

MODELING PROCEDURE

Numerical electromagnetic (EM) simulations were performed using the finite element method implemented on the COMSOL Multiphysics platform, as described in the Supporting Information. Simulations were carried out on periodic (periodicity = 570 nm) square arrays of idealized structures: a cross with a thickness of 100 nm and gammadion structures with variable thickness, h = 5, 30, and 100 nm, as shown in Figure 1a,b. The cross and gammadion in free space

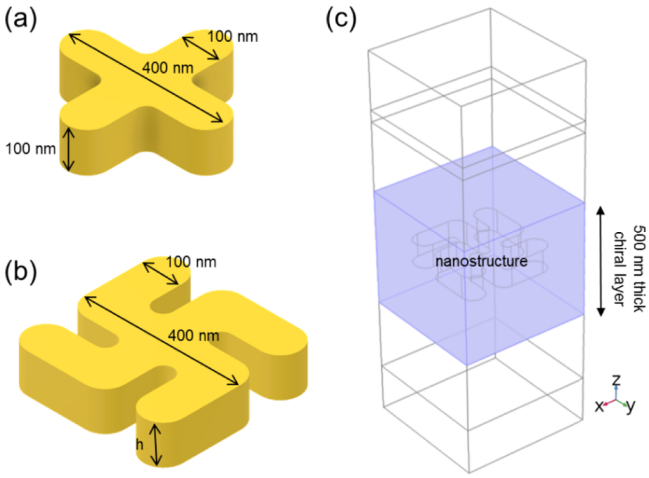

Figure 1. Simulated idealized cross (a) and gammadion (b) structures belonging to the D_{4h} and C_{4h} point groups, respectively. The gammadion structures studied had variable heights of h = 5, 30, and 100 nm. (c) Model unit cell showing the position of the nanostructure and the 500 nm thick chiral layer.

belong to D_{4h} and C_{4h} point groups, respectively. Both shapes possess a planar symmetry, however, the cross also contains vertical mirror planes. Although the gammadion is achiral, its two planar surfaces are intrinsically left- and right-handed. Thus, the surface plasmons associated with these interfaces will be chiral. Using a chemical analogy, one can consider a gammadion to be a diastereomer composed of L- and D-component parts. Subsequently, we will refer to the two interfaces of the gammadion as left (L) and right (R) faces, as shown in Figure 2. The convention used for assignment of handedness is the same as that used in previous work.[5,9] Both cross and gammadion structures have been modeled when embedded into nonadsorbing isotropic achiral and chiral dielectrics of refractive index 1.523. The approach for modeling a chiral dielectric has been described elsewhere.[17]

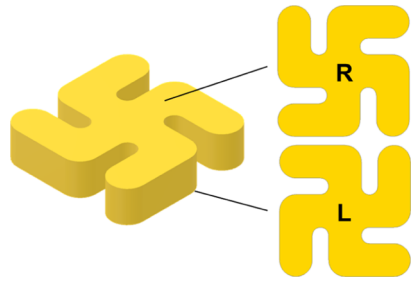

Figure 2. Idealized gammadion with right (R)- and left (L)-handed faces identified.

For completeness, a brief description of the approach will now be given. The effect of chiral dielectric media on optical properties is modeled using the constitutive equations for a chiral medium[4]

$$\mathcal{D} = \varepsilon_0\varepsilon_r\mathcal{E} + i\xi^{iso}\mathcal{B} \quad (1)$$

$$\mathcal{H} = \mathcal{B}/\mu_0\mu_r + i\xi^{iso}\mathcal{E} \quad (2)$$

Here, ε_0 is the permittivity of free space, ε_r is the relative permittivity, μ_0 is the permeability of free space, μ_r is the relative permeability, $\mathcal{E}$ is the complex electric field, $\mathcal{B}$ is the complex magnetic flux density, $\mathcal{H}$ is the magnetic field, $\mathcal{D}$ is the electric displacement field, and ξ^{iso} is a second rank tensor describing the chiral property of a molecular layer. ξ^{iso} is only nonzero for a chiral dielectric. The sign of the pseudoscalar tensor elements ξ^{iso}_{ij} (i, j = x, y & z) is defined by the handedness of the chiral dielectric. For an isotropic chiral medium, only electric-dipole−magnetic dipole interactions contribute significantly to the asymmetry in optical responses.[18] In this case only the diagonal elements of the chirality tensor, ξ^{iso} are nonzero, with

$$\xi^{iso} = \begin{bmatrix} \xi^{iso}_{xx} & 0 & 0 \\ 0 & \xi^{iso}_{yy} & 0 \\ 0 & 0 & \xi^{iso}_{zz} \end{bmatrix} \quad (3)$$

where

$$\xi^{iso}_{xx} = \xi^{iso}_{yy} = \xi^{iso}_{zz} \quad (4)$$

We simulated nanostructures embedded in this isotropic chiral layer, of thickness 500 nm (Figure 1c), and with $\xi^{iso}_{xx,yy,zz} = 10^{-4}$ which is the value expected for isotropic chiral material which displays CD in the near UV.[4] Using a previous convention,[17] a positive value of the tensor elements models a right-handed material.

Simulations have been performed for both left and right CPL (LCP/RCP) incident on the L and R faces of the gammadion structure (i.e., four combinations) as well as on the cross on its two planar faces.

SIMULATED PARAMETERS: CD SPECTRA, OPTICAL CHIRALITY, OPTICAL CHIRALITY FLUXES

CD spectra have been derived from the differential transmission of LCP and RCP light (see the Supporting Information). To aid comparison with previous experimental work, CD spectra are displayed in units of milli-degrees, rather than quoted in terms of absolute differences of transmission.

DOI: 10.1021/acs.jpcc.9b02791
J. Phys. Chem. C 2019, 123, 15195−15203

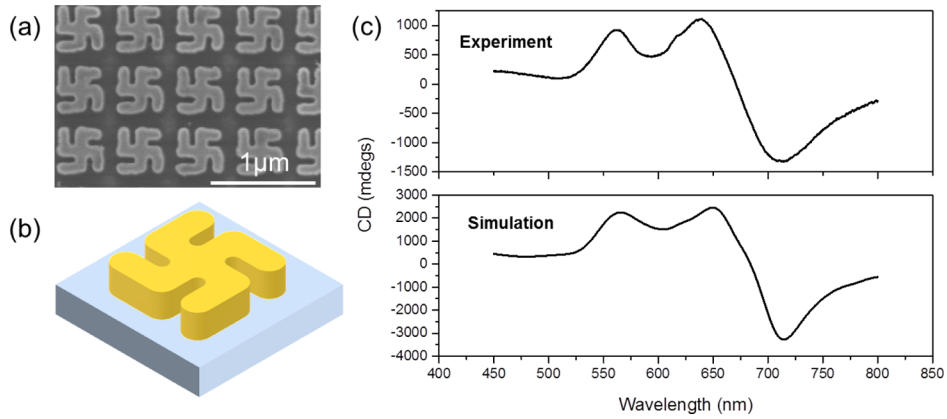

Figure 3. (a,b) Comparison of an electron micrograph of the fabricated structures and the modeled structure. (c) Comparison of experimental (top panel) and simulated (bottom panel) CD spectra.

The chiral asymmetry of near fields can be parameterized using an optical chirality parameter C, first proposed by Tang and Cohen[19] and defined as follows

$$C = \frac{\varepsilon_0}{2}\boldsymbol{E}\cdot\nabla\times\boldsymbol{E} + \frac{1}{2\mu_0}\boldsymbol{B}\cdot\nabla\times\boldsymbol{B} \tag{5}$$

where $\boldsymbol{E}$ and $\boldsymbol{B}$ are the time-dependent electric and magnetic fields, respectively. By analogy with Poynting's theorem, the following expression can be derived for optical chirality flux ($\boldsymbol{F}$)

$$\frac{\partial C}{\partial t} + \frac{1}{\mu}\nabla\cdot\boldsymbol{F} = -\frac{1}{2}(\boldsymbol{j}\cdot\nabla\times\boldsymbol{E} + \boldsymbol{E}\cdot\nabla\times\boldsymbol{j}) \tag{6}$$

where $\boldsymbol{j}$ are material currents and

$$\boldsymbol{F} = \frac{1}{2}[\boldsymbol{E}\times(\nabla\times\boldsymbol{B}) - \boldsymbol{B}\times(\nabla\times\boldsymbol{E})] \tag{7}$$

Given that chirality is a conserved quantity,[12,15,16,20] the implication of eq 6 is that material currents can act as a source or sink of optical chirality. Thus, the chiralities of EM fields and electronic motion can be interconverted. From the numerical simulations, we determine both the time-averaged optical chirality of the near field $\overline{C}$ and optical chirality flux $\overline{\boldsymbol{F}}$ transmitted. It has previously been demonstrated that $\overline{\boldsymbol{F}}$ is proportional to the level of circular polarization measured in the far field.[16] Thus, a reduction in $\overline{\boldsymbol{F}}$ relative to that of CPL indicates a level of depolarization.

RESULTS

Validating Modeling Procedure. The robustness of our modeling methodology has been validated through comparison with experimental CD data obtained from nanofabricated arrays in air. Right-handed Au gammadions with a thickness of 100 nm, arm widths of 100 nm, and periodicity of 570 nm were fabricated on a glass substrate, the fabrication strategy is outlined in the Supporting Information. A comparison of the modeled structure and an electron micrograph of the nanofabricated structure is shown in Figure 3a,b. The simulated and experimental spectra Figure 3c are in good agreement, albeit with some differences. The modeled spectra do show both slightly larger levels of ellipticity (factor of ~2) and narrower resonances than the experimental data. The difference in the level of ellipticity is due to the strategy employed during the fabrication of the experimental arrays. One millimeter square areas which contain the nanostructures are arranged in a "checkerboard" formation such that only half of the substrate is covered. This was done to reduce fabrication time. Small differences in the resonance shape can be attributed to structural defects that are not accounted for in the idealized structure including structural imperfections which break the fourfold symmetry and surface roughness. The very good agreement between the experiment and modeled spectra validates the efficacy of our modeling methodology for nanoparticles.

Achiral Dielectric. As would be expected, crosses embedded in an achiral dielectric do not produce CD and the simulations are independent of which the planar face the LCP and RCP are incident on (see the Supporting Information).

A CD signal is observed for all gammadion thicknesses, as shown in Figure 4. The sign of the CD spectra is dependent on

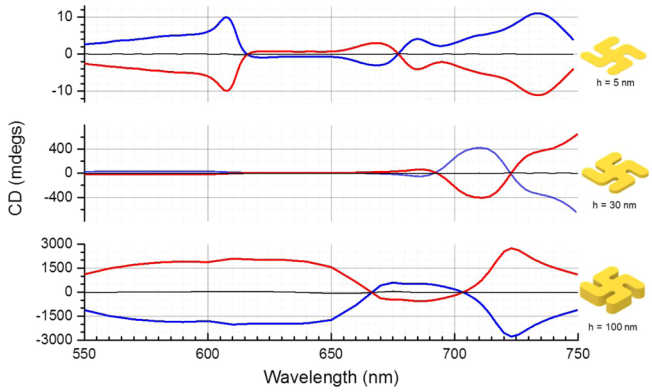

Figure 4. Simulated CD spectra for gammadions of h = 5 nm, (top panel), 30 nm (middle panel), and 100 nm (bottom panel) when light is incident upon their right (blue) and left (red) faces. Their mean is shown in black and is ~0 in all cases.

the handedness of the planar surface light is incident upon. The 5 nm structure shows the smallest CD signal, more than an order of magnitude smaller than the 30 nm thick structure which in turn shows a maximum CD signal 5 times smaller than the 100 nm thick structure. Because CD spectra for light incident upon the L and R faces display equal and opposite behavior, the mean of the two spectra (shown in black) is equal to zero. The implication of this is that if the gammadions and crosses were freely floating in a liquid (i.e., have isotropic

DOI: 10.1021/acs.jpcc.9b02791
J. Phys. Chem. C 2019, 123, 15195−15203

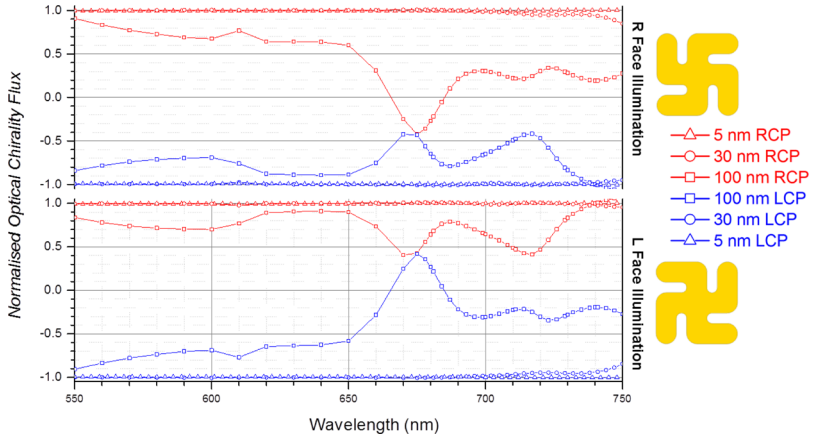

Figure 5. Optical chirality flux plots for h = 5 nm thick (triangles), 30 nm thick (circles), and 100 nm thick (squares) gammadions suspended in an achiral medium illuminated with RCP (red) and LCP (blue) on the R (top panel) and L (bottom panel) faces.

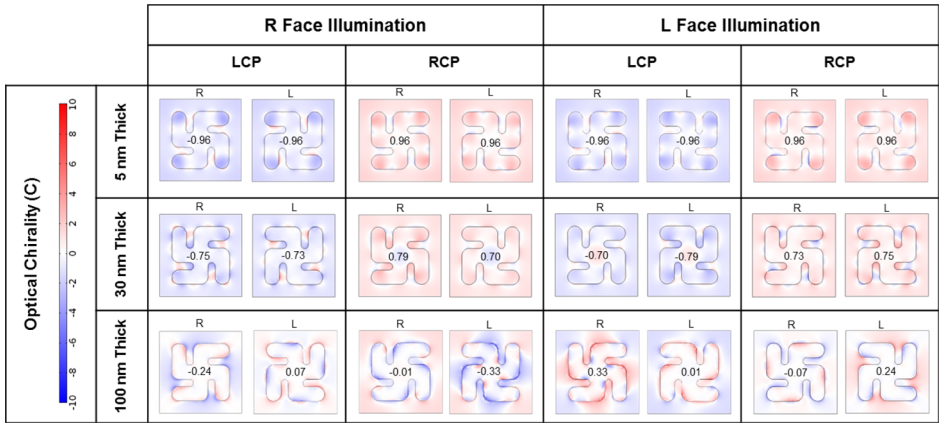

Figure 6. Optical chirality maps on the R and L faces for h = 5, 30, and 100 nm thick gammadions suspended in an achiral medium illuminated with RCP and LCP on their opposite faces. The integrated chirality value across the surface is shown in the centre of the diagram.

distributions of orientations with respect to the light propagation direction), no CD signal would be observed in either case as would be expected for an achiral structure.

The observation of a nonreciprocal CD from the achiral gammadions structures can be easily rationalized. If the gammadion was uniformly excited, no optical activity would be observed. This is because L and R faces would exhibit equal and opposite behavior to CPL, thus resulting in no net CD. This can only occur if $h \ll$ Au attenuation (absorption) length λ_{Au}, otherwise optical absorption will lead to nonuniform fields across the structure. For the wavelength range studied 550−750 nm, λ_{Au} = 17.7−13.3 nm respectively, hence the condition $h \ll \lambda_{Au}$ is not met for the h values modeled.

By analogy with CD in molecular systems, one would intuitively attribute the increase in the magnitude of the CD with h, to higher levels of absorption because of the greater quantity of Au. However, this simplistic interpretation is inconsistent with the relative levels of optical absorption of the three simulated structures. Based on a mean λ_{Au} of ∼15 nm across the wavelength range studied, the amount of incident light absorbed by the structures would be ∼100, 87, and 29%, respectively, for h = 100, 30, and 5 nm thick structures (see the Supporting Information for electric field plots and calculation of absorption). These values are inconsistent with the relative magnitudes of CD for the three thicknesses which is approximately 150:40:1.

To provide insight into the h dependency of the chiroptical properties, we have derived optical chirality flux spectra for the gammadions structures, as shown in Figure 5 for incident LCP and RCP. The transmitted optical chirality fluxes ($\bar{F}$) have been normalized to that of RCP of equivalent intensities, thus, $\|\bar{F}\| < 1$ indicates a dissipation of chirality by the structure. For all structures, the $\bar{F}$ spectra display the expected behavior for chiral systems; enantiomeric pairs (combinations of light and gammadion face which are related by mirror symmetry) display equal and opposite behavior. For instance, LCP incident on the L face is the mirror image of RCP incident on the R face. There is little dissipation of optical chirality, and hence depolarization, for h = 5 and 30 nm. However, there is a dramatic change for the h = 100 nm gammadion. There is a significant dissipation of optical chirality over the whole wavelength range for all combinations. However, the greatest level of dissipation is for the RCP (LCP) and R (L) combinations. Indeed, the sign of the optical fluxes reverse in these cases over the 665−685 nm range.

Plots showing the spatial extent and optical chiralities of the near fields, at the wavelength of the maximum CD, are displayed in Figure 6. For ease of comparison, we have also included the integrated average optical chirality value for a given surface in the centre of each diagram.

The behavior of near-field optical chirality mimics the trend observed for $\bar{F}$. For h = 5 nm, the sign of the optical chirality is

DOI: 10.1021/acs.jpcc.9b02791
J. Phys. Chem. C 2019, 123, 15195−15203

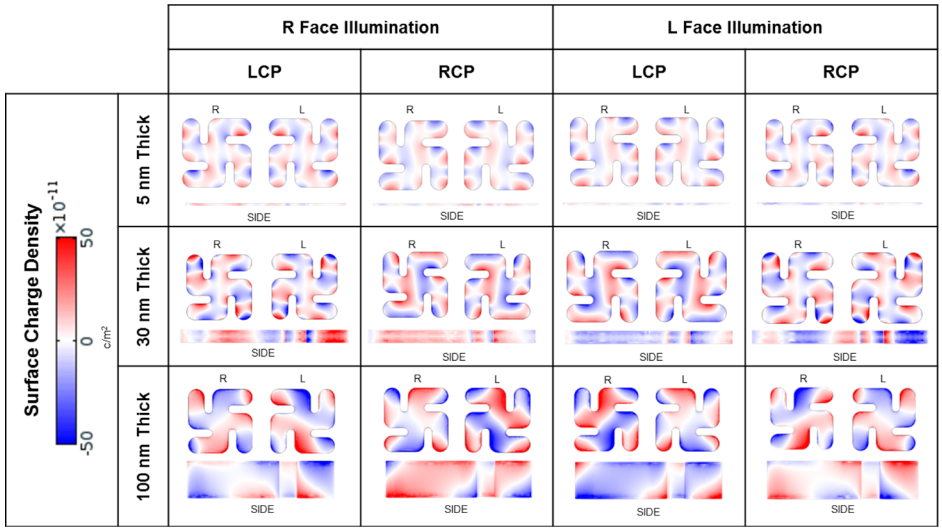

Figure 7. Surface charge density maps on the R and L faces for h = 5, 30, and 100 nm gammadions suspended in an achiral medium illuminated with RCP and LCP on their opposite faces.

almost completely that of the polarization of the incident light. There are "superchiral" regions of the near field with a maximum $|\overline{C}|$ of ∼6 on average, but there are also areas where $|\overline{C}| < 1$. The data for h = 30 nm show differences to that for h = 5 nm. The $\overline{C}$ of the majority of the near-field region has the same sign as that of the incident light. However, there are regions with opposite sign, which are most pronounced for R/RCP and L/LCP combinations. Once again, there are regions with $|\overline{C}| > 1$ and $|\overline{C}| < 1$; with the average maximum value of $|\overline{C}| \approx 5$. As with $\overline{\boldsymbol{F}}$ data, there is a significant change in the h = 100 nm plots. Now, the near fields have significant regions with $\overline{C}$ of opposite signs to that of the incident light with the average maximum $|\overline{C}| \approx 8$.

Given that chirality is a conserved quantity,[12,15,16,20] the changes observed in both $\overline{C}$ and $\overline{\boldsymbol{F}}$ must be offset by a commensurate change in the chirality of the electron distributions of the plasmonic structure. This is validated by the simulation of the (instantaneous) surface charge distributions. From these, deductions can be made on the level of symmetry breaking induced by the time-averaged surface charge densities.

In Figure 7 are surface charge density plots at the maxima CD positions for gammadion structures for each combination of polarization and surface handedness. The plots show the surface charge densities on both the planar faces and on the side walls. The plots for side walls are taken from the same face (looking down the y-axis, see the Supporting Information) to aid comparison. As expected, the chiral asymmetry of the charge distributions increases with h. Polarization and surface-handedness combinations which are enantiomeric display mirror symmetric charge distributions.

For h = 5 nm, all four polarization and light incidence combinations produce overall charge distributions on the L and R faces which are almost identical; while for h = 30 nm, they are also similar but display a 180° phase difference. These simulations indicate that for both 5 and 30 nm, the time-averaged charge distributions on the L and R faces will be very similar. For both 5 and 30 nm, the charge distributions on the side walls display only a very weak asymmetry with respect to the horizontal mirror plane of the gammadion. Thus, if the symmetry of the gammadion is considered in terms of the surface charge distribution, then, for the 5 and 30 nm case, there is only a slight chiral perturbation to lift the horizontal mirror symmetry. This contrasts with the results for h = 100 nm in which there are distinctly different surface charge distributions on the L and R faces, and distributions on the side wall break the horizontal mirror of the gammadion structure. Consequently, for h = 100 nm, the time-averaged surface charge distribution acts as a significant chiral perturbation lifting the horizontal mirror plane of the gammadion.

Consequently, the simulations of $\overline{C}$, $\overline{\boldsymbol{F}}$ and surface charge densities are consistent with the effective conversion between optical and electronic chiralities for h = 100 nm: an increase in the dissipation of optical chirality results in a commensurate increase in chiral currents; thus greater asymmetries in surface charge distributions.

It has previously been proposed that optical chirality can be dissipated through loss (i.e., absorption) and at interfaces.[16] The dependency of the dissipation of optical chirality on h is inconsistent with the two mechanisms. The loss mechanism can be ruled out based on the fact that optical chirality dissipation does not scale linearly with the predicted levels of absorption for the three h values. Equally, if the interface mechanism was responsible for the observed effect, dissipation of optical chirality would scale with the surface area of the gammadion, which it does not.

We propose a previously unconsidered mechanism by which optical chirality can be dissipated and that would be consistent with the dependence on h. Specifically, we suggest that optical chirality can be dissipated through an interference mechanism. The model assumes that the two oppositely handed faces of a gammadion act as spatially separated sources of chiral near fields which can interfere both with each other and light incident upon the structures, the result of which is that the optical chirality flux $\overline{\boldsymbol{F}}$ is dependent on the phase differences between the two sources and incident light.

The proposed model assumes $\boldsymbol{\mathcal{E}}$ and $\boldsymbol{\mathcal{B}}$ are the net complex time-harmonic electric and magnetic fields. We can then express $\boldsymbol{\mathcal{E}}$ and $\boldsymbol{\mathcal{B}}$ as the sum of fields generated by incident light and the oppositely handed faces of the structure

DOI: 10.1021/acs.jpcc.9b02791
J. Phys. Chem. C 2019, 123, 15195−15203

$$\mathcal{E} = \mathcal{E}_I + \mathcal{E}_L e^{i\theta} + \mathcal{E}_R e^{i\varphi} \quad (8)$$

$$\mathcal{B} = \mathcal{B}_I + \mathcal{B}_L e^{i\theta} + \mathcal{B}_R e^{i\varphi} \quad (9)$$

where $\mathcal{B}_I$ and $\mathcal{E}_I$ are the fields of the incident light; $\mathcal{B}_L$, $\mathcal{E}_L$, $\mathcal{B}_R$, and $\mathcal{E}_R$ are the fields generated by the left- and right-handed faces. θ and φ are the relative phases of the fields at the left- and right-handed faces relative to the incident light. Using eqs 7, 8, and 9, the following expression for transmitted real optical chirality flux can be derived for an arbitrary helicity of light

$$\bar{F} = (\bar{F}_{II} + \bar{F}_{LL} + \bar{F}_{RR}) + 2(\bar{F}_{IL}\cos\theta + \bar{F}_{IR}\cos\varphi + \bar{F}_{LR}\cos(\varphi - \theta)) + 2(\bar{G}_{IL}\sin\theta + \bar{G}_{IR}\sin\varphi + \bar{G}_{LR}\sin(\varphi - \theta)) \quad (10)$$

where $\bar{F}_I$, $\bar{F}_L$, and $\bar{F}_R$ are time averaged optical chirality fluxes of the incident light and left- and right-handed faces in isolation. The remaining terms in eq 10 account for interferences between the incident light and the two sources. A full derivation of eq 10 is given in the Supporting Information. The expression establishes the link between $\bar{F}$ and phase: it implicitly suggests that optical chirality can be dissipated through an interference mechanism involving relative changes in the phase.

Up to this point, we have considered $\bar{F}$ in generic terms for any light polarization and face incidence. We now specify the optical chirality flux in terms of the face of incidence where L Inc and R Inc denote light incidence on left- and right-handed surfaces. For an achiral dielectric, ${}^{\mathrm{LCP}}_{\mathrm{L\ Inc(R\ Inc)}}\bar{F}$ and ${}^{\mathrm{RCP}}_{\mathrm{R\ Inc(L\ Inc)}}\bar{F}$ are enantiomeric pairs and are related by

$${}^{\mathrm{LCP}}_{\mathrm{L\ Inc(R\ Inc)}}\bar{F} = -{}^{\mathrm{RCP}}_{\mathrm{R\ Inc(L\ Inc)}}\bar{F} \quad (11)$$

From this, further enantiomeric pair relationships for the terms in eq 10 can be derived

$${}^{\mathrm{LCP(RCP)}}_{\mathrm{L\ Inc(R\ Inc)}}\theta = {}^{\mathrm{RCP(LCP)}}_{\mathrm{R\ Inc(L\ Inc)}}\varphi \quad (12)$$

$${}^{\mathrm{LCP(RCP)}}_{\mathrm{R\ Inc(L\ Inc)}}\theta = {}^{\mathrm{RCP(LCP)}}_{\mathrm{L\ Inc(R\ Inc)}}\varphi \quad (13)$$

$${}^{\mathrm{LCP(RCP)}}_{\mathrm{L\ Inc(R\ Inc)}}\bar{F}_L = -{}^{\mathrm{RCP(LCP)}}_{\mathrm{R\ Inc(L\ Inc)}}\bar{F}_R \quad (14)$$

$${}^{\mathrm{LCP(RCP)}}_{\mathrm{R\ Inc(L\ Inc)}}\bar{F}_L = -{}^{\mathrm{RCP(LCP)}}_{\mathrm{L\ Inc(R\ Inc)}}\bar{F}_R \quad (15)$$

$${}^{\mathrm{LCP}}\bar{F}_I = -{}^{\mathrm{RCP}}\bar{F}_I \quad (16)$$

Equations 12 and 13 express the enantiomeric relationships for the interference terms in eq 10. Further, for the proposed simple interference model, the following relationship holds

$$2\pi\frac{hn}{\lambda} = (\theta - \varphi) \quad (17)$$

where n is the refractive index of the surrounding medium, λ is the wavelength of light, and h is the height of the nanostructure. Equation 17 correlates the increase in the height of the nanostructure with an increase in the phase difference generated by its two faces.

To summarize, we propose that eq 10 is the basis of an interference mechanism for the dissipation of optical chirality. The mechanism is analogous to the case of energy flux, where interference suppresses radiative emission, with material currents acting as an energy reservoir. In this case, material currents instead act as a reservoir for chirality. The increase in the levels of CD with h can be rationalized within this framework. As h increases, so do the values of $\theta - \varphi$ and θ or φ (depending on the face of incidence) leading to an increase in the dissipation of optical chirality.

Therefore, when combined, eqs 10 and 17 imply an increase in optical chirality flux dissipation with increasing h. This results in higher levels of chiral material currents within the structure. We propose that this "injection" of electronic chirality increases the level of CD. Put simply, LCP (RCP) is more strongly dissipated than RCP (LCP) when incident on an L (R) structure. This effectively amplifies the L (R) chiral asymmetry of the electrons, thus increasing the CD.

Chiral Dielectric. The introduction of the chiral dielectric induces a CD in the cross (Figure 8) which is reciprocal with respect to the direction of propagation of light: that is, it is the same irrespective of the propagation direction. This replicates qualitatively the experimental observation of chiral induction by molecular chiral layers in plasmonic crosses[21] and nano-islands.[22] The wavelength position of the induced chiral plasmon in the simulation is consistent with both of these experimental observations. However, the level of the CD in the simulation is larger by an order of magnitude than in the cross experiment. This can partly be attributed to a number of factors: (a) the cross was not completely surrounded by a chiral dielectric; (b) the chiral dielectric film was thinner in the experiment; (c) the experimental samples were fabricated in a checkerboard pattern as previously described.

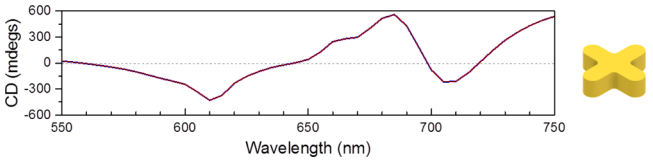

Figure 8. Simulated CD spectrum for the cross structure encapsulated by chiral media. CD is identical for light incident on both the faces.

For gammadions, the effects of the chiral dielectric are dependent on the nanostructure thickness (Figure 9). In the h = 5 nm thick case, there is a background due to chiral induction which is comparable to the magnitude of the inherent CD of the nanostructure. This induced CD background has resonances at ≈615 and 670 nm. These are

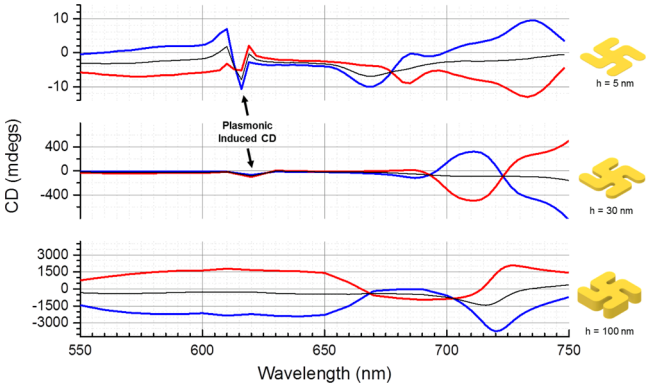

Figure 9. CD spectra for the gammadion structures encapsulated by a chiral layer when light is incident on its R (blue) and L (red) faces. The mean of the two incidences is shown in black. A plasmonic-induced CD resonance is identified in the h = 5 and 30 nm structures.

DOI: 10.1021/acs.jpcc.9b02791
J. Phys. Chem. C 2019, 123, 15195−15203

in similar regions to the features induced in the cross structure. When this background is taken into account, there is minimal asymmetry in the positions of the inherent CD resonances of the structure. This background has less of an influence on the spectra of the two thicker structures because of the significantly larger magnitude of the inherent CD resonances.

In the case of h = 30 nm, apart from the induced feature, the presence of the chiral dielectric does not cause any significant changes to the spectra, such as asymmetric shifts in resonance positions. The presence of a chiral dielectric has the most dramatic influence on the behavior of the h = 100 gammadion structures. There are significant asymmetry shifts (∼8 nm) in the intrinsic CD resonances of the gammadions. This qualitatively replicates previous observations of chiral molecular sensing.[5,7] The mean replicates the spectra for the detection of phenylalanine enantiomers using arrays of racemic gammadions.[8] There is no discernible chiral dielectric-induced CD resonance. This can be assigned to the fact that an intense intrinsic CD peak of the gammadions occurs in the same region, which masks the less-intense induced peak.

The $\overline{F}$ spectra, as shown in Figure 10, display a similar dependency on h as the CD data. For h = 5 and 30 nm

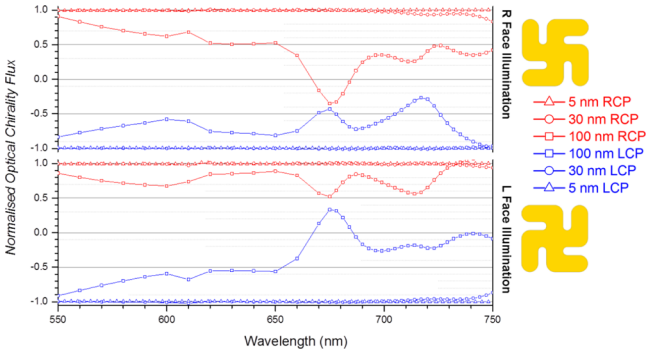

Figure 10. Optical chirality flux plots for 5 nm thick (triangles), 30 nm thick (circles), and 100 nm thick (squares) gammadions suspended in a chiral medium illuminated with RCP (red) and LCP (blue) on the R (top panel) and L (bottom panel) faces.

structures, the chiral dielectric induces a new feature at ∼610 nm which coincides with the induced CD peak. The new feature does not display mirror image behavior between enantiomeric pair combinations of face handedness and CPL. However, the presence of the chiral dielectric does not significantly change the spectra in the rest of the wavelength range, with spectra of enantiomeric pair combinations displaying almost mirror symmetry. The behavior for h = 100 nm is significantly different, with a complete breakdown of the mirror symmetry between spectra of enantiomeric pair combinations. Specifically, the chiral dielectric enables LCP to be more and RCP to be less effectively dissipated relative to the achiral electric.

The $\overline{C}$ plots calculated at the wavelength of the maximum CD, as shown in Figure 11, are very similar to those for the achiral dielectric, with no significant change in sign or spatial distribution. There is a change in magnitude of the near field which is consistent with the greater efficiency of dissipating LCP observed in the $\overline{F}$ spectra. This can be illustrated by considering the averaged integrated $\overline{C}$ value of the near fields for h = 100 nm. For instance, the LCP/R $\overline{C}$ values for the achiral and chiral dielectrics are −0.24 and −0.22, indicating enhanced dissipation leading to lower $\overline{C}$ in the near field. In the case of the corresponding enantiomeric pair (RCP/L), the achiral and chiral $\overline{C}$ values are 0.24 and 0.26, showing a reduced level of dissipation.

Therefore, the chiral dielectric simulations qualitatively replicate two previously reported phenomena: (a) the molecular layer induced chiral induction in plasmonic particles; and (b) chiral molecular sensing with chiral plasmonic particles. The data clearly demonstrate that the sensing capabilities of the particles are not directly correlated to the maximum magnitude of $\overline{C}$. However, the sensing capability is correlated to h and hence by implication the interference mechanism.

Consequently, we propose a mechanism for enantiomer sensing in which the phases, θ and φ, are asymmetrically changed by the presence of a chiral dielectric. Central to this assumption is that the presence of the chiral dielectric breaks the symmetry of the system, and hence ${}^{\mathrm{LCP}}_{\mathrm{L\,Inc(R\,Inc)}}\overline{F}$ and ${}^{\mathrm{RCP}}_{\mathrm{R\,Inc(L\,Inc)}}\overline{F}$ are no longer enantiomeric pairs. Thus,

$$ {}^{\mathrm{LCP}}_{\mathrm{L\,Inc(R\,Inc)}}\overline{F} \neq -{}^{\mathrm{RCP}}_{\mathrm{R\,Inc(L\,Inc)}}\overline{F} \tag{18} $$

and consequently, the relationships in 11 no longer hold. Equation 16 still hold if the surrounding dielectric is nonlossy. The refractive index of a chiral material (n_{chiral}) is given by

$$ n_{\mathrm{chiral}} = n \pm \delta n \tag{19} $$

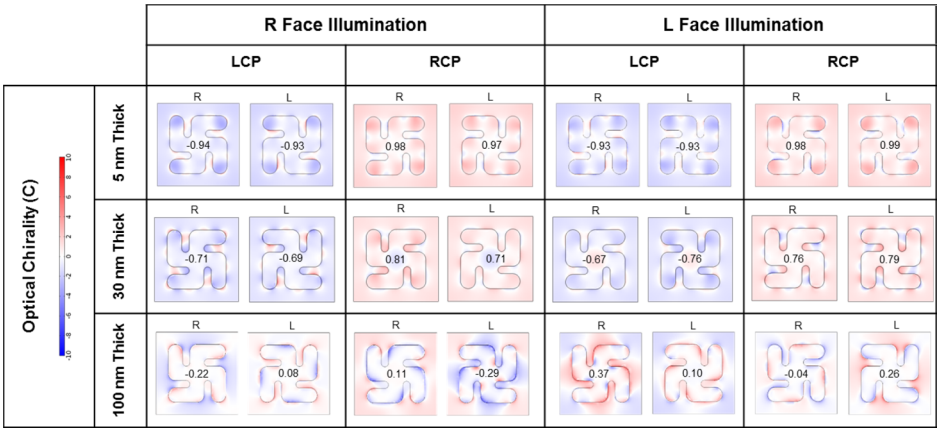

Figure 11. Optical chirality maps on the R and L faces for h = 5, 30, and 100 nm thick gammadions suspended in a chiral medium illuminated with RCP and LCP on their two planar faces. The integrated chirality values across the surface are shown in the centre of the diagram.

DOI: 10.1021/acs.jpcc.9b02791
J. Phys. Chem. C 2019, 123, 15195−15203

where n is the refractive index of a racemic (achiral) mixture and the sign of δn is governed by the handedness of the scattered light. This means that eq 17 is modified to

$$2\pi\frac{h(n \pm \delta n)}{\lambda} = (\theta - \varphi) \tag{20}$$

From this relation, it is clear that

$$^{\mathrm{LCP}}_{\mathrm{L\ Inc(R\ Inc)}}(\theta - \varphi) \neq {}^{\mathrm{RCP}}_{\mathrm{R\ Inc(L\ Inc)}}(\theta - \varphi) \tag{21}$$

which in turn leads to the asymmetric behavior expressed in the data in Figures 10 and 11.

Interference between emissions between neighboring structures could also contribute to the dissipation of chirality. To assess the contribution this makes to the observed asymmetry, simulations of individual (nonperiodic) nanostructures have been performed (see the Supporting Information). These simulations exhibit asymmetries in CD comparable to those observed in the periodic structures. Consequently, interference between structures does not play a dominant role in producing the asymmetric behavior.

SUMMARY

Fundamentally, the core concept explored in this study is that interference can suppress the levels of optical chirality radiated into the far field. Hence, interference can be considered a mechanism for optical chirality dissipation. Our work demonstrates that chiral sensing is derived from this interference phenomenon. This is consistent with the previously reported observation of enantiomer detection with plasmonic-induced transparency in chiral plasmonic structures.[17,23] Consequently, this study provides a framework for the rational design of chiral plasmonic materials for sensing applications. Optimizing the level of enhanced chirality (superchirality) of the near field is not a sufficient condition to produce effective enantiomer detection. Useful sensing structures must be engineered to display interference effects. Near fields with enhanced optical chirality, "*superchirality*", will amplify the asymmetries in the phase differences required for sensing.

This work also indicates that free-floating nanoparticles would be effective sensors in solutions of biological molecules: the mean of R and L face illumination is nonzero, therefore, randomly oriented nanoparticles surrounded by chiral molecules would show a CD signal. This would provide a useful tool for providing a biomolecular structure in vitro.

ASSOCIATED CONTENT

Supporting Information

The Supporting Information is available free of charge on the ACS Publications website at DOI: 10.1021/acs.jpcc.9b02791.

EM simulation methods and calculations, fabrication information, electric field plots for the structures, CD spectra for periodic crosses and isolated 100 nm thick gammadions, and derivation of equations (PDF)

AUTHOR INFORMATION

Corresponding Authors

*E-mail: c.gilroy.1@research.gla.ac.uk (C.G.).
*E-mail: shun.hashiyada@riken.jp (S.H.).
*E-mail: malcolm.kadodwala@glasgow.ac.uk (M.K.).

ORCID

Shun Hashiyada: 0000-0002-3229-538X
Affar S. Karimullah: 0000-0002-8792-9829
Hiromi Okamoto: 0000-0003-0082-8652
Malcolm Kadodwala: 0000-0003-4989-5688

Notes

The authors declare no competing financial interest.

ACKNOWLEDGMENTS

The authors acknowledge financial support from the Engineering and Physical Sciences Research Council EP/M024423/1), JSPS Core to Core programme and technical support from the James Watt Nanofabrication Centre (JWNC). C.G. work was supported by the EPSRC CDT in Intelligent Sensing and Measurement, Grant Number EP/L016753/1.

REFERENCES

(1) Barron, L. D. *Molecular Light Scattering and Optical Activity*, 2nd ed.; Cambridge University Press, 2004.
(2) Kelly, S. M.; Jess, T. J.; Price, N. C. How to Study Proteins by Circular Dichroism. *Biochim. Biophys. Acta, Proteins Proteomics* **2005**, *1751*, 119−139.
(3) Yoo, S.; Park, Q.-H. Metamaterials and Chiral Sensing: A Review of Fundamentals and Applications. *Nanophotonics* **2019**, *8*, 249−261.
(4) Kelly, C.; Tullius, R.; Lapthorn, A. J.; Gadegaard, N.; Cooke, G.; Barron, L. D.; Karimullah, A. S.; Rotello, V. M.; Kadodwala, M. Chiral Plasmonic Fields Probe Structural Order of Biointerfaces. *J. Am. Chem. Soc.* **2018**, *140*, 8509−8517.
(5) Hendry, E.; Carpy, T.; Johnston, J.; Popland, M.; Mikhaylovskiy, R. V.; Lapthorn, A. J.; Kelly, S. M.; Barron, L. D.; Gadegaard, N.; Kadodwala, M. Ultrasensitive Detection and Characterization of Biomolecules Using Superchiral Fields. *Nat. Nanotechnol.* **2010**, *5*, 783−787.
(6) Tullius, R.; Karimullah, A. S.; Rodier, M.; Fitzpatrick, B.; Gadegaard, N.; Barron, L. D.; Rotello, V. M.; Cooke, G.; Lapthorn, A.; Kadodwala, M. "Superchiral" Spectroscopy: Detection of Protein Higher Order Hierarchical Structure with Chiral Plasmonic Nanostructures. *J. Am. Chem. Soc.* **2015**, *137*, 8380−8383.
(7) Zhao, Y.; Askarpour, A. N.; Sun, L.; Shi, J.; Li, X.; Alù, A. Chirality Detection of Enantiomers Using Twisted Optical Metamaterials. *Nat. Commun.* **2017**, *8*, 14180.
(8) García-Guirado, J.; Svedendahl, M.; Puigdollers, J.; Quidant, R. Enantiomer-Selective Molecular Sensing Using Racemic Nanoplasmonic Arrays. *Nano Lett.* **2018**, *18*, 6279−6285.
(9) Khoo, E. H.; Leong, E. S. P.; Wu, S. J.; Phua, W. K.; Hor, Y. L.; Liu, Y. J. Effects of Asymmetric Nanostructures on the Extinction Difference Properties of Actin Biomolecules and Filaments. *Sci. Rep.* **2016**, *6*, 19658.
(10) Bliokh, K. Y.; Nori, F. Characterizing Optical Chirality. *Phys. Rev. A: At., Mol., Opt. Phys.* **2011**, *83*, 021803.
(11) Tang, Y.; Cohen, A. E. Enhanced Enantioselectivity in Excitation of Chiral Molecules by Superchiral Light. *Science* **2011**, *332*, 333−336.
(12) Lipkin, D. M. Existence of a New Conservation Law in Electromagnetic Theory. *J. Math. Phys.* **1964**, *5*, 696−700.
(13) Schäferling, M.; Dregely, D.; Hentschel, M.; Giessen, H. Tailoring Enhanced Optical Chirality: Design Principles for Chiral Plasmonic Nanostructures. *Phys. Rev. X* **2012**, *2*, 031010.
(14) Hendry, E.; Mikhaylovskiy, R. V.; Barron, L. D.; Kadodwala, M.; Davis, T. J. Chiral Electromagnetic Fields Generated by Arrays of Nanoslits. *Nano Lett.* **2012**, *12*, 3640−3644.
(15) Vázquez-Lozano, J. E.; Martínez, A. Optical Chirality in Dispersive and Lossy Media. *Phys. Rev. Lett.* **2018**, *121*, 043901.
(16) Poulikakos, L. V.; Gutsche, P.; McPeak, K. M.; Burger, S.; Niegemann, J.; Hafner, C.; Norris, D. J. Optical Chirality Flux as a Useful Far-Field Probe of Chiral Near Fields. *ACS Photonics* **2016**, *3*, 1619−1625.

DOI: 10.1021/acs.jpcc.9b02791
J. Phys. Chem. C 2019, 123, 15195−15203

(17) Kelly, C.; Khosravi Khorashad, L.; Gadegaard, N.; Barron, L. D.; Govorov, A. O.; Karimullah, A. S.; Kadodwala, M. Controlling Metamaterial Transparency with Superchiral Fields. *ACS Photonics* **2018**, *5*, 535.
(18) Govorov, A. O.; Fan, Z. Theory of Chiral Plasmonic Nanostructures Comprising Metal Nanocrystals and Chiral Molecular Media. *ChemPhysChem* **2012**, *13*, 2551−2560.
(19) Tang, Y.; Cohen, A. E. Optical Chirality and Its Interaction with Matter. *Phys. Rev. Lett.* **2010**, *104*, 163901.
(20) Philbin, T. G. Lipkin's Conservation Law, Noether's Theorem, and the Relation to Optical Helicity. *Phys. Rev. A: At., Mol., Opt. Phys.* **2013**, *87*, 043843.
(21) Abdulrahman, N. A.; Fan, Z.; Tonooka, T.; Kelly, S. M.; Gadegaard, N.; Hendry, E.; Govorov, A. O.; Kadodwala, M. Induced Chirality through Electromagnetic Coupling between Chiral Molecular Layers and Plasmonic Nanostructures. *Nano Lett.* **2012**, *12*, 977−983.
(22) Maoz, B. M.; Chaikin, Y.; Tesler, A. B.; Bar Elli, O.; Fan, Z.; Govorov, A. O.; Markovich, G. Amplification of Chiroptical Activity of Chiral Biomolecules by Surface Plasmons. *Nano Lett.* **2013**, *13*, 1203−1209.
(23) Tullius, R.; Platt, W.; Khorashad, L. K.; Gadegaard, N.; Lapthorn, A. J.; Rotello, V. M.; Cooke, G.; Barron, L. D.; Govorov, A. O.; Karimullah, A. S.; Kadodwala, M. Superchiral Plasmonic Phase Sensitivity for Fingerprinting of Protein Interface Structure. *ACS Nano* **2017**, *11*, 12049−12056.

DOI: 10.1021/acs.jpcc.9b02791
J. Phys. Chem. C 2019, 123, 15195−15203